ELSEVIER

Materials Science and Engineering A 478 (2008) 56–64

MATERIALS SCIENCE & ENGINEERING A

www.elsevier.com/locate/msea

Fatigue crack propagation behavior of friction stir welded 5083-H32 and 6061-T651 aluminum alloys

Sangshik Kim [a,*], Chang Gil Lee [b], Sung-Joon Kim [b]

[a] *School of Nano and Advanced Materials Engineering, Engineering Research Institute, Gyeongsang National University, Chinju 660-701, Republic of Korea*

[b] *Institute of Materials Science and Technology, Korea Institute of Machinery and Materials, Changwon 641-831, Republic of Korea*

Received 28 October 2006; received in revised form 16 May 2007; accepted 7 June 2007

Abstract

The fatigue crack propagation (FCP) behavior of FSWed 5083-H32 and 6061-T651 specimens were examined with the fatigue crack growing either parallel to the dynamically recrystallized zone (DXZ) at variable ΔK values and an R ratio of 0.1 and 0.8, respectively, or perpendicular or 45° to the DXZ at various constant ΔK values and an R ratio of 0.1. Residual stress was measured on the top surface of FSWed plate either perpendicular or parallel to the welding direction and the residual stress-corrected ΔK, ΔK_{corr}, is calculated based on the K_{res}, the stress intensity factor at residual stress, for the DXZ specimens to quantify the compressive residual stress contribution to the FCP rates. The present study suggests that the FCP behavior of FSWed 5083-H32 and 6061-T651 specimens in the DXZ is mainly determined by the beneficial compressive residual stress reducing effective ΔK and the detrimental grain refinement causing intergranular fatigue failure. The FCP behavior of FSWed 5083-H32 and 6061-T651 specimens is discussed based on residual stress measurement and fractographic observation.

Keywords: 5083-H32; 6061-T651; Friction stir welding; Fatigue crack propagation

1. Introduction

Friction stir welding (FSW) is a new solid-state joining method offering several advantages over conventional welding methods, including better mechanical properties, low residual stress and reduced occurrence of defects [1–4]. The tensile strength and tensile elongation of FSWed 5083-H32 specimen are, for example, 301 MPa and 17% compared to 306 MPa and 22% for the base metal (BM) specimen [5]. The tensile strength of FSWed 6061-T651 specimen is approximately 20% lower than that for the BM specimen with similar to better tensile ductility [6]. The resistance to corrosion and stress corrosion cracking for the FSWed specimen in 3.5% NaCl aqueous solution is better or comparable to the BM due to grain refinement in the weld zone [7].

The FSW technique for joining aluminum alloys now reaches the early stage of commercial usage particularly in the aerospace and automotive industries [8–10]. Despite the practical significance, relatively little research has been conducted on fatigue crack propagation (FCP) behavior of FSWed aluminum alloys [11–14]. It has been proposed that the FCP behavior of FSWed aluminum alloys is strongly influenced by grain refinement in the dynamically recrystallized zone (DXZ) and/or the residual stress developed in the FSW zone [11,12]. A controversy exists for the FCP behavior of FSWed aluminum alloys. Pao et al. proposed that compressive residual stresses lower the crack-tip driving force (ΔK) in the DXZ resulting in lower FCP rates and higher apparent ΔK_{th} in FSWed 2519 alloy [11]. Jata et al., on the other hand, suggested that fine recrystallized grains formed in the weld zone dominate the FCP behavior of FSWed 7050-T7451 alloy and reduce the resistance to FCP [12].

The objective of this study is to examine the FCP behavior of FSWed 5083-H32 and 6061-T651 aluminum alloys. 5083-H32 and 6061-T651 alloys are excellent all round aluminum alloys ideal for many applications including transportation and construction [15–17]. The FCP rates for FSWed 5083-H32 and 6061-T651 specimens were measured with the fatigue crack growing either parallel to the DXZ at variable ΔK and at an

* Corresponding author. Tel.: +82 55 751 5309; fax: +82 55 762 8670.
E-mail address: sang@gsnu.ac.kr (S. Kim).

0921-5093/$ – see front matter © 2007 Elsevier B.V. All rights reserved.
doi:10.1016/j.msea.2007.06.008

R ratio of 0.1 and 0.8, respectively, or perpendicular or 45° to the DXZ at various constant ΔK values at an *R* ratio of 0.1. The FCP behavior of FSWed 5083-H32 and 6061-T651 Al alloys were discussed based on the micrographic and fractographic observation and residual stress measurement.

2. Experimental procedure

Four millimeter thick 5083-H32 and 6061-T651 aluminum alloy plates were used for friction stir welding in this study. It was previously reported that the best tool rotating speed and welding speed combination is 1600 rpm/0.25 mpm (m/min.) for the FSWed 5083-H32 specimen and 1200 rpm/0.2 mpm for the FSWed 6061-T651 specimen considering tensile strength and ductility [5,6]. The tool geometry used in this study is the same as the one used in references [5,6]. Table 1 represents the tensile properties of the BM and the FSWed 5083-H32 and 6061-T651 specimens. Cross-sectional macro and micrographs were documented by optical microscope for 5083-H32 specimen etched with modified Poulton's reagent (40 ml HNO_3 + 12 g H_2CrO_4 + 30 ml HCl + 2.5 ml HF + 42.5 ml H_2O) and for 6061-T651 specimen etched with Dix and Keller's reagent (6 ml HNO_3 + 3 ml HCl + 6 ml HF + 150 ml H_2O). For quantitative grain size measurement, electron backscatter diffraction (EBSD) technique was used. Fig. 1 shows (a) the optical macrograph and the EBSD images for the FSWed 5083-H32 specimen in the (b) dynamically recrystallized zone (DXZ), (c) thermomechanically affected zone (TMAZ), and (d) base metal (BM), respectively, cross-sectioned perpendicular to the welding direction. Fig. 2 shows (a) the macroscopic optical micrograph and the EBSD images for the FSWed 6061-T651 specimen in the (b) DXZ, (c) TMAZ, and (d) BM, respectively. Table 2 summarizes the grain

Table 1
Tensile properties of the BM and the FSWed 5083-H32 and 6061-T651 specimens

Alloy	Condition	Yield strength (MPa)	Ultimate tensile strength (MPa)	Tensile elongation (%)
5083-H32	BM	137	306	22.0
	FSWed	150	301	17.0
6061-T651	BM	246	311	14.7
	FSWed	144	231	13.0

Table 2
Average grain sizes (μm) for the BM, TMAZ and DXZ, respectively, for the FSWed 5083-H32 and 6061-T651 specimens

Alloy	BM	TMAZ	DXZ
5083-H32	19.0	16.1	8.2
6061-T651	25.3	20.2	8.6

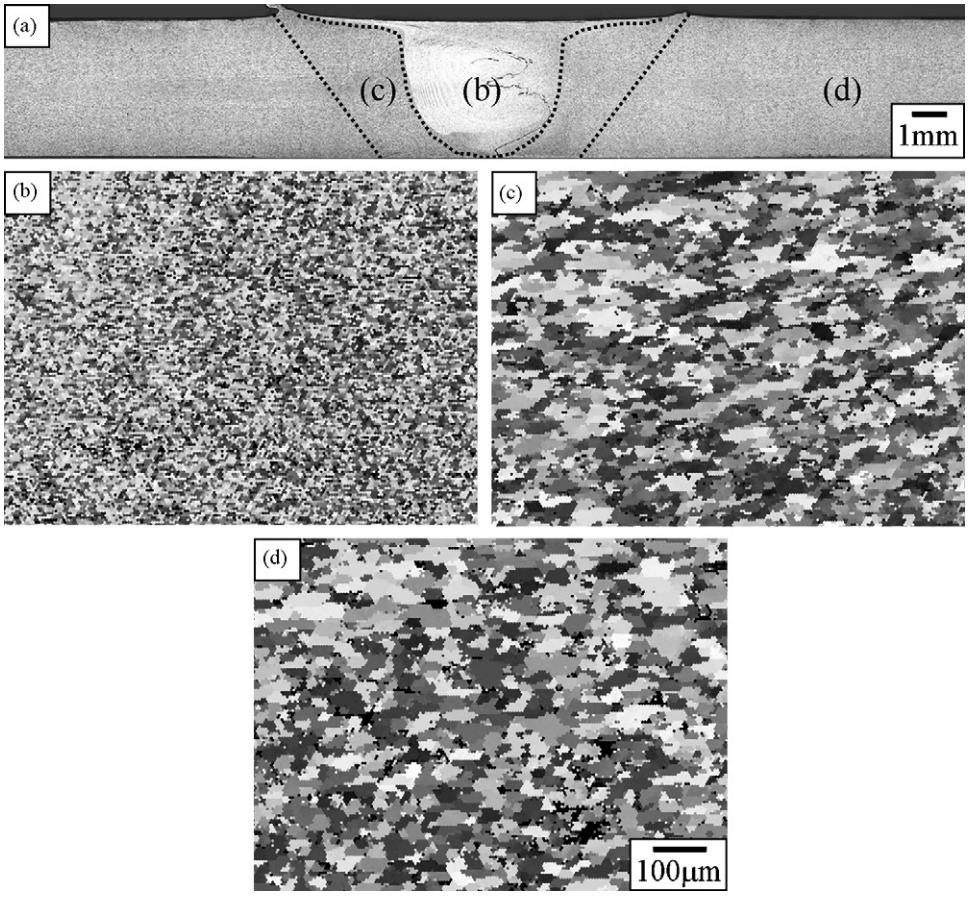

Fig. 1. Typical (a) macroscopic optical micrograph and the EBSD images for the FSWed 5083-H32 specimen in the (b) dynamically recrystallized zone (DXZ), (c) thermomechanically affected zone (TMAZ), and (d) base metal (BM), respectively, cross-sectioned perpendicular to the welding direction.

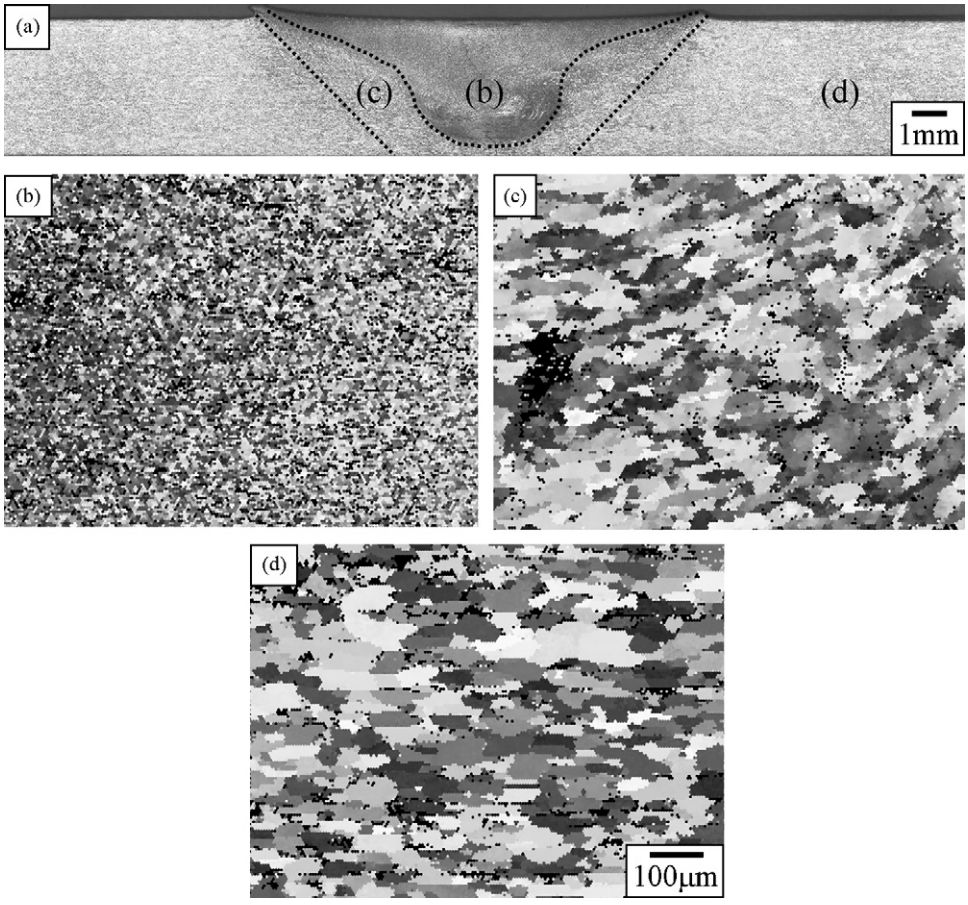

Fig. 2. Typical (a) macroscopic optical micrograph and the EBSD images for the FSWed 6061-T651 specimen in the (b) DXZ, (c) TMAZ, and (d) BM, respectively.

size measurement for each zone obtained from Figs. 1 and 2 showing that the DXZ has much finer grain structure compared to the BM due to dynamic recrystallization during FSW process. The standard deviation for the grain size measurement in this study was ±10%.

Compact tension (CT) specimens with a width (W) of 50.8 mm and a thickness (B) of 4.0 mm were prepared from the FSWed plate for both alloy specimens. Two different types of FCP tests were conducted in this study. First, the FCP tests were conducted at an R (stress) ratio of 0.1 and 0.8, respectively, and a sinusoidal frequency of 10 Hz with the fatigue crack growing along the DXZ at variable ΔK values. The second set of FCP tests were performed with the crack either perpendicular or 45° to the DXZ at various constant ΔK values at an R ratio of 0.1. The cracks propagated from the advancing side to the retreating side of the DXZ. Fig. 3 shows the schematic illustration of CT specimens used for (a) the FCP test at variable ΔK values with the crack parallel to the DXZ, and for the test at constant ΔK with the crack (b) perpendicular and (c) 45°, respectively, to the DXZ. The FCP rates were measured by using a DCPD (direct current potential drop) technique. Residual stress analyses were performed on the top surface of FSWed plate either perpendicular or parallel to the welding direction using Rigaku model D/MAX-3C X-ray diffractometer. The fractographs for the fatigue fractured specimens were examined by using scanning electron microscope (SEM).

3. Results and discussion

Previously, it was proposed that the FCP behavior of FSWed aluminum alloys is strongly influenced by grain refinement and residual stress developed near the FSW zone [11,12]. A number of studies have reported that compressive residual stress develops both longitudinal and transverse to the weld in the FSWed specimen due to complex thermal and rigid clamping used during FSW process [13,14]. Fig. 4 shows transverse (perpendicular to the welding direction) and longitudinal (parallel to the welding direction) residual stress distribution for the FSWed 5083-H32 (Fig. 4(a and b)) and the FSWed 6061-T651 (Fig. 4(c and d)) specimens as a function of distance from the weld center. The negative side from the weld center represents the advancing side of the nugget. Fig. 4(a) indicates that average compressive residual stress of approximately 19 MPa exists within the weld zone ranging approximately ±10 mm from the weld center perpendicular to the welding direction for both alloy specimens. Along the welding direction (Fig. 4(b)), maximum compressive residual stress of approximately 30 MPa is observed on the advancing side of the 5083-H32 weld, which is approximately 12 mm away from the weld center. The optical micrographic observation suggests that this region with maximum residual stress showed no microstructural difference compared to the BM (Fig. 5) and is designated as residual stress affected zone (RSAZ) in this study. Unlike the advancing side, negligible ten-

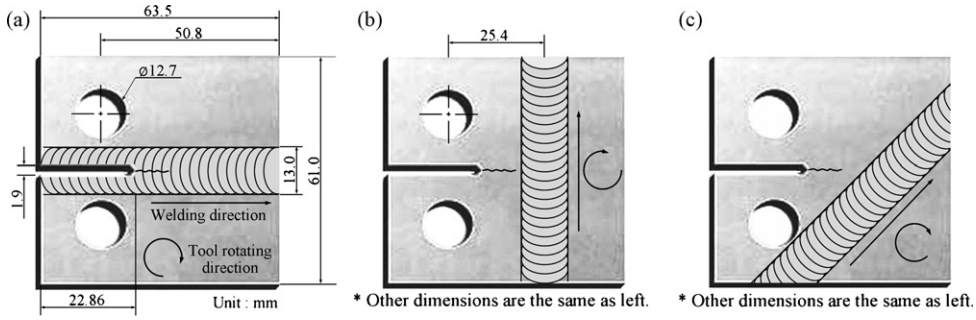

Fig. 3. Schematic illustration of CT specimens used for (a) the FCP test at variable ΔK values with the crack growing parallel to the DXZ, and for the test at constant ΔK with the crack growing (b) perpendicular and (c) 45°, respectively, to the DXZ.

sile or compressive residual stress was noted on the retreating side. The FSWed 6061-T651 specimens also show similar residual stress distribution for those observed in the FSWed 5083-H32 specimens.

In order to understand the effects of refined microstructure in the DXZ and the residual stress on the FCP behavior of FSWed 5083-H32 and 6061-T651 specimens, two different types of fatigue crack growth tests were conducted. First, the FCP rates for FSWed 5083-H32 and 6061-T651 specimens were measured with the fatigue crack growing along the BM and the DXZ, respectively, at variable ΔK values and an R ratio of 0.1 and 0.8, respectively. The second type of fatigue test consists of fatigue crack growing either perpendicular or 45° to the welding direction at various constant ΔK values. Fig. 6 shows the da/dN–ΔK curves for the FSWed (a) 5083-H32 and (b) 6061-T651 specimens along the BM and the DXZ, respectively, at an R ratio of 0.1 and 0.8, respectively. The FCP rates for the DXZ specimens were substantially lower than those for the BM over the entire stress intensity factor range studied at an R ratio of 0.1 for both 5083-H32 and 6061-T651 specimens. The FCP rate retardation is particularly significant in low and intermediate ΔK regimes. The reduced FCP rates in low ΔK regime for the DXZ specimen were also noted at an R ratio of 0.8 for both alloy specimens. The enhanced resistance to FCP at an R ratio of 0.8 for the DXZ specimen is, however, not as significant as that at an R ratio of 0.1. At a high R ratio of 0.8 and in the intermediate and high ΔK regimes, the DXZ and BM specimens showed similar FCP rates for both alloy specimens.

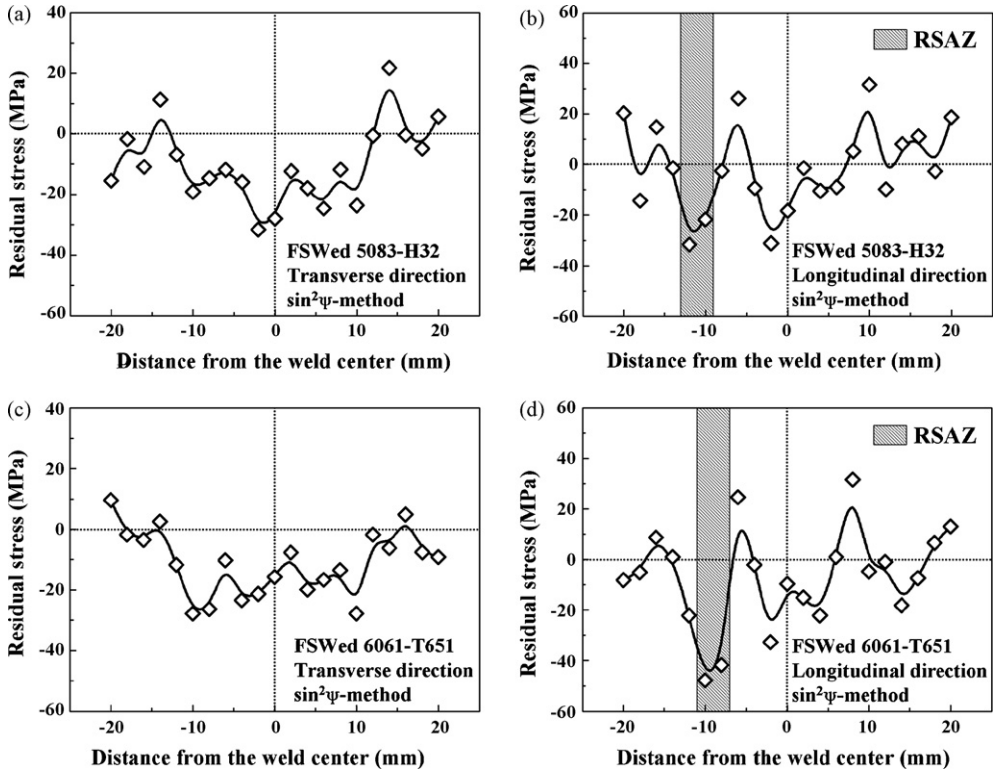

Fig. 4. Residual stress distribution for the (a), (b) FSWed 5083-H32 and (c), (d) 6061-T651 specimens either along the transverse (perpendicular to the welding direction) or longitudinal (parallel to the welding direction) direction as a function of distance from the weld center. The RSAZ represents residual stress affected zone.

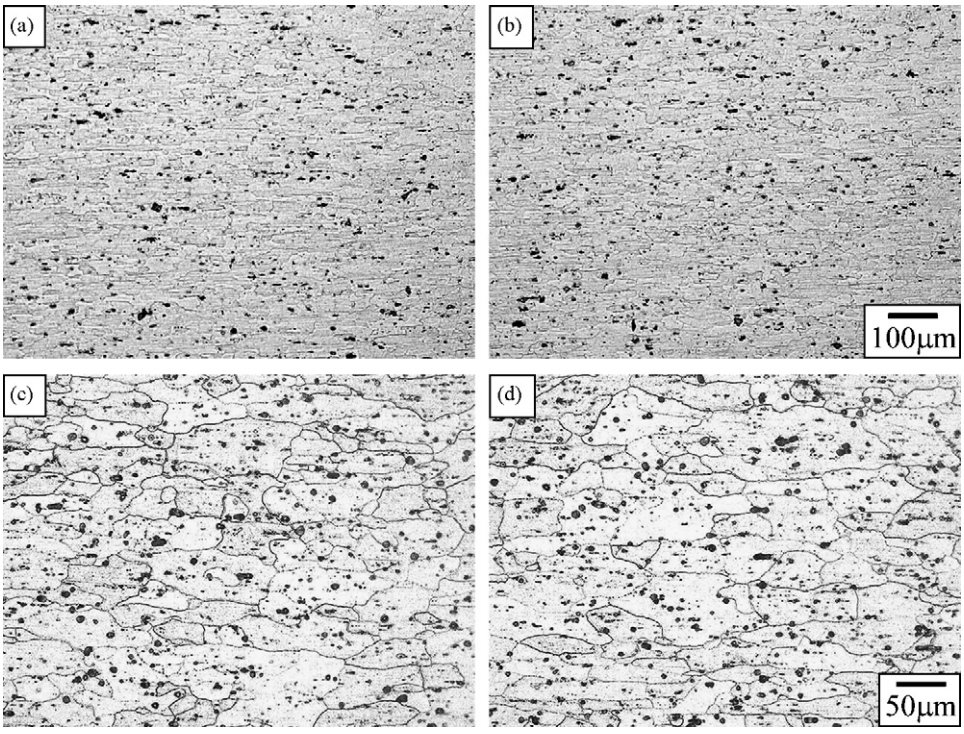

Fig. 5. Optical micrographs of FSWed 5083-H32 and 6061-T651 specimens in the (a) 5083-H32 BM, (b) FSWed 5083-H32 RSAZ, (c) 6061-T651 BM, and (d) FSWed 6061-T651 RSAZ, respectively.

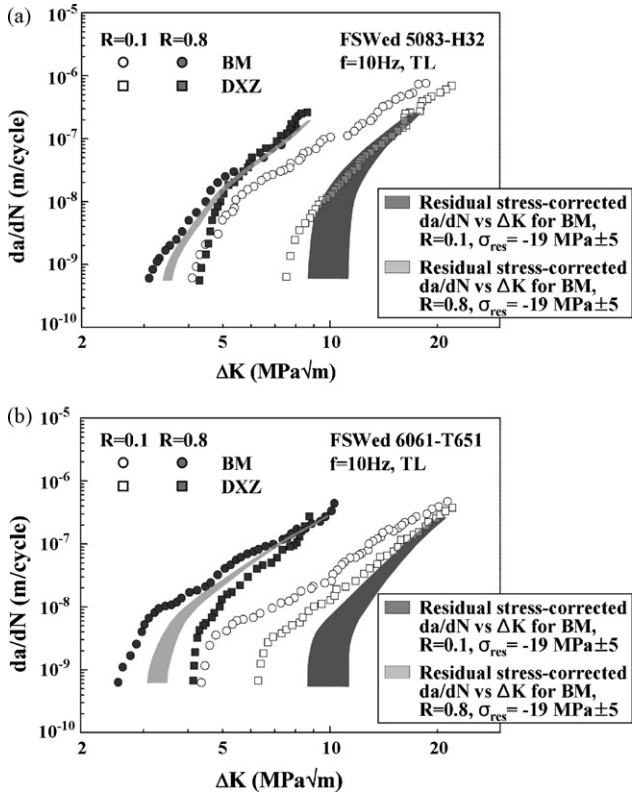

Fig. 6. da/dN–ΔK curves for the FSWed (a) 5083-H32 and (b) 6061-T651 specimens along the BM and the DXZ, respectively, at an R ratio of 0.1 and 0.8, respectively.

As represented in Fig. 4(a and c), the average compressive residual stress of approximately 19 MPa for both FSWed 5083-H32 and 6061-T651 specimens exists in the DXZ perpendicular to the crack propagation direction and this would decrease the FCP rates by reducing the effective ΔK. In order to quantify the compressive residual stress contribution to the FCP rates, the residual stress-corrected ΔK, ΔK_{corr}, is calculated based on the K_{res}, the stress intensity factor at residual stress, for the DXZ specimens. The residual stress-corrected da/dN–ΔK relationship was calculated, as follows. The stress intensity factor at residual stress, K_{res}, is calculated using [18,19]:

$$K_{res} = \sigma_{res}\sqrt{W}\frac{(2+\alpha)}{(1-\alpha)^{3/2}}(0.886 + 4.64\alpha - 13.32\alpha^2 + 14.72\alpha^3 - 5.6\alpha^4) \quad (1)$$

where K is the stress intensity factor, σ_{res} the residual stress, W the specimen width, $\alpha = a/W$, and a is the crack length.

To utilize K_{res} factors in crack growth predictions, effective stress intensity factor range, ΔK_{eff}, is defined as [20]

$$\Delta K_{eff} = (K_{max} + K_{res}) - (K_{min} + K_{res}) = \Delta K_{app} \quad (2)$$

where K_{max} is the maximum stress intensity factor, K_{min} the minimum stress intensity factor, and ΔK_{app} is the applied stress intensity factor range.

If $K_{min} + K_{res}$ is greater than zero, the corrected stress intensity factor range is taken as [20]

$$\Delta K_{corr} = \Delta K_{eff} = \Delta K_{app} \quad (3)$$

where ΔK_{corr} is the corrected stress intensity factor range, and ΔK_{eff} is the effective stress intensity factor range and if

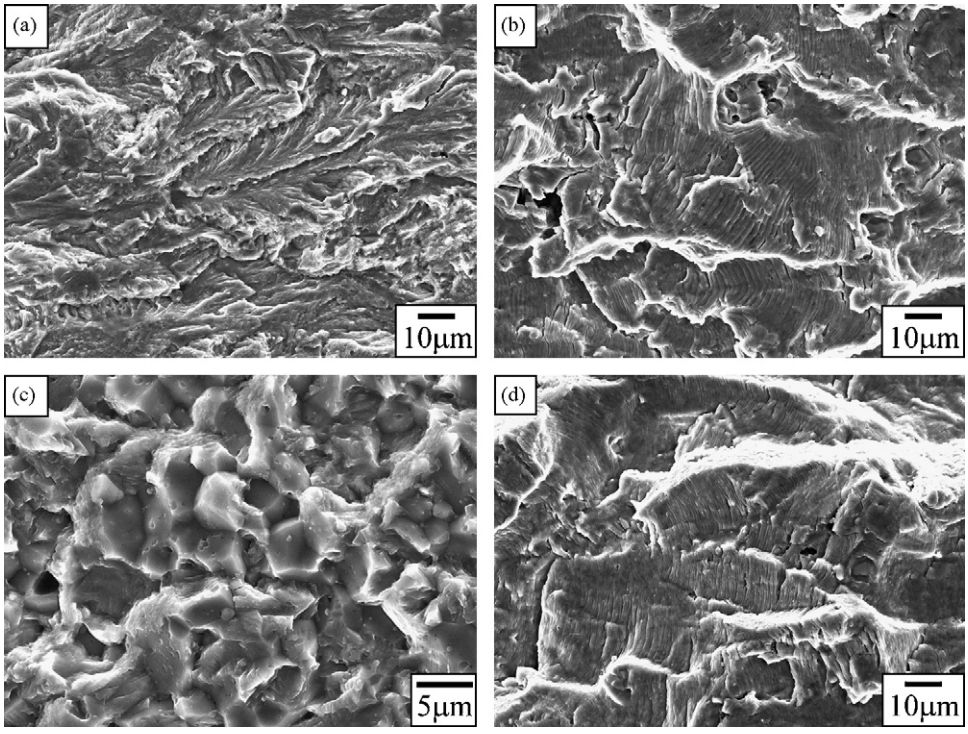

Fig. 7. SEM fractographs of the FSWed 5083-H32 specimens fatigued along the BM at (a) $\Delta K \approx 4\,\mathrm{MPa}\sqrt{\mathrm{m}}$ and (b) $\Delta K \approx 20\,\mathrm{MPa}\sqrt{\mathrm{m}}$, respectively, and the DXZ at (c) $\Delta K \approx 7.5\,\mathrm{MPa}\sqrt{\mathrm{m}}$ and (d) $\Delta K \approx 20\,\mathrm{MPa}\sqrt{\mathrm{m}}$, respectively.

$K_{\min} + K_{\mathrm{res}}$ is lower than zero, then an effective R ratio becomes zero, and [20]

$$\Delta K_{\mathrm{corr}} = \Delta K_{\mathrm{app}} - K_{\mathrm{res}} \tag{4}$$

For an R ratio of 0.1 in the present study, the K_{res} value is calculated based on the σ_{res} of -19 ± 5 MPa. The $K_{\min} + K_{\mathrm{res}}$ is then lower than zero and ΔK_{corr} becomes $\Delta K_{\mathrm{eff}} - K_{\mathrm{res}}$ with an effective R ratio of zero. At a high R ratio of 0.8, $K_{\min} + K_{\mathrm{res}}$ is

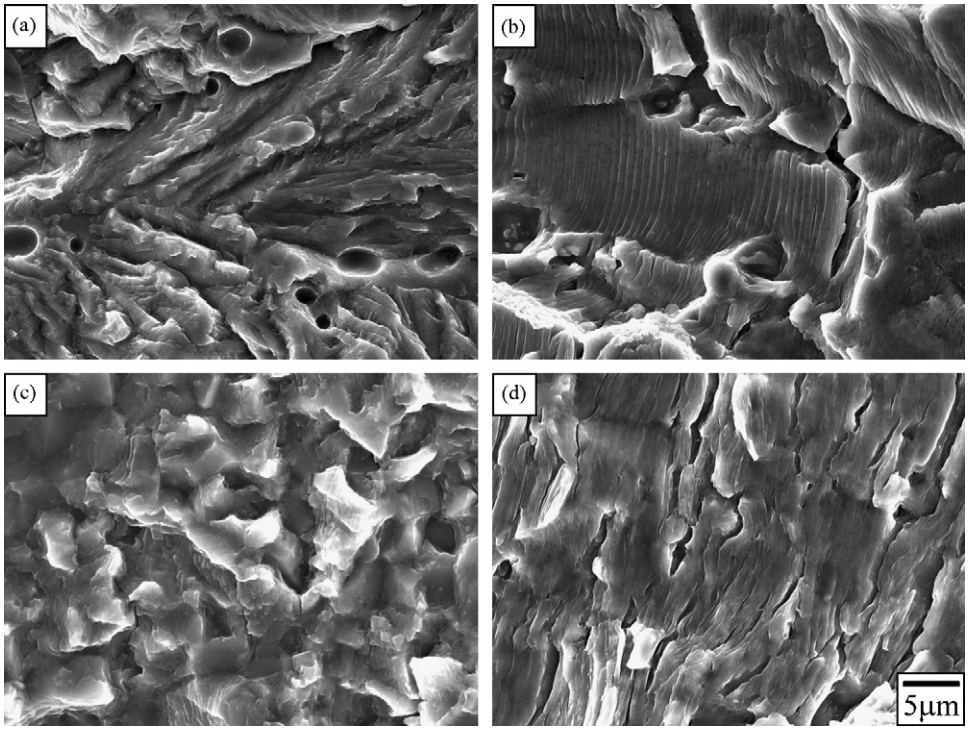

Fig. 8. SEM fractographs of the FSWed 6061-T651 specimens fatigued along the BM at (a) $\Delta K \approx 5\,\mathrm{MPa}\sqrt{\mathrm{m}}$ and (b) $\Delta K \approx 20\,\mathrm{MPa}\sqrt{\mathrm{m}}$, respectively, and the DXZ at (c) $\Delta K \approx 7\,\mathrm{MPa}\sqrt{\mathrm{m}}$ and (d) $\Delta K \approx 20\,\mathrm{MPa}\sqrt{\mathrm{m}}$, respectively.

greater than zero and ΔK_{corr} is the same as ΔK_{corr} with reduced effective R ratios varying from 0.4 to 0.8. The da/dN–ΔK_{corr} bands for the DXZ specimens at an R ratio of 0.1 and 0.8, respectively, are presented in Fig. 6, showing that the corrected FCP rates with residual stress do not match to those for the DXZ specimens. At an R ratio of 0.1, the residual stress-corrected FCP rates are substantially lower than those for the DXZ specimens in the low ΔK regime for both 5083-H32 and 6061-T651 specimens, suggesting that residual stress alone cannot explain the reduced FCP rates in the DXZ at an R ratio of 0.1. Previously, Jata et al. proposed that fine recrystallized grains formed in the DXZ could increase the FCP rates of the FSWed 7075-T7451 specimen by reducing crack closure contribution [12]. As shown in Table 2, the average grain size of the DXZ for the FSWed 5083-H32 and 6061-T651 specimen is approximately 40 and 35%, respectively, smaller than that for the BM specimen. It is therefore reckoned that the discrepancy between the residual stress-corrected FCP rates and the FCP rates for the DXZ specimen in the low ΔK regime is due to the reduced crack closure contribution with refined microstructure. Figs. 7 and 8 show the SEM fractographs of 5083-H32 specimens (Fig. 7) and 6061-T651 specimens (Fig. 8) fatigued at an R ratio of 0.1 along the BM (a) in the near-threshold ΔK regime and (b) at high applied ΔK value of approximately 20 MPa$\sqrt{m}$, respectively, and the DXZ (c) in the near-threshold ΔK regime and (d) $\Delta K \approx 20$ MPa$\sqrt{m}$, respectively. Unlike the typical cleavage facet for the BM specimen (Figs. 7(a) and 8(a)), intergranular FCP mode was noted for the DXZ specimen in the near-threshold ΔK regime (Figs. 7(c) and 8(c)). Such an intergranular fatigue crack path caused by grain refinement in the near-threshold ΔK regime would further reduce the resistance to FCP [21]. In high ΔK regime, both specimens showed crystallographic facet fracture mode showing no notable difference. At a high R ratio of 0.8, the crack closure contribution is expected to be minimal. Without crack closure contribution at this R ratio, the residual stress-corrected da/dN–ΔK_{corr} curve obtained from the BM data roughly matches to da/dN–ΔK for the DXZ specimen for both alloy specimens. At an R ratio of 0.8, the $\Delta K_{th,corr}$ values appears to be slightly lower than those for the DXZ specimen for both alloy specimens. Considering that the intergranular fatigue crack path at an R ratio of 0.8 and in the near-threshold ΔK regime (see Fig. 9(a) for the FSWed 5083-H32 specimen at $\Delta K \approx 4.3$ MPa$\sqrt{m}$ and Fig. 9(b) for the FSWed 6061-T651 specimen at $\Delta K \approx 4.2$ MPa$\sqrt{m}$) reduces the resistance to FCP, other microstructural features than the reduced grain size for the DXZ specimen may affect the intrinsic FCP behavior of both alloy specimens. The increased dislocation density during friction stir welding in the DXZ [22,23], for example, may restrict the motion of dislocations emitted from a crack-tip and eventu-

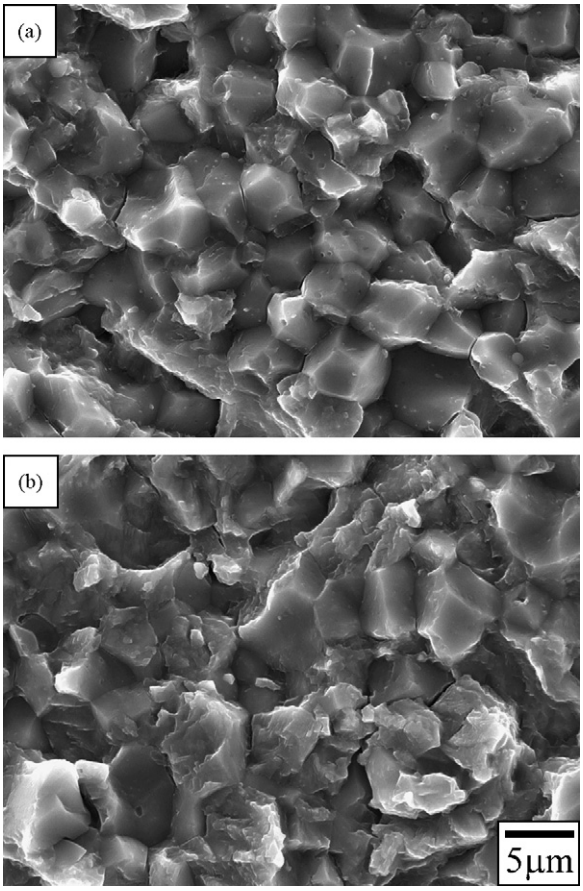

Fig. 9. SEM fractographs of the FSWed (a) 5083-H32 and (b) 6061-T651 specimen, respectively, fatigued at an R ratio of 0.8 along the DXZ in the near-threshold ΔK regime.

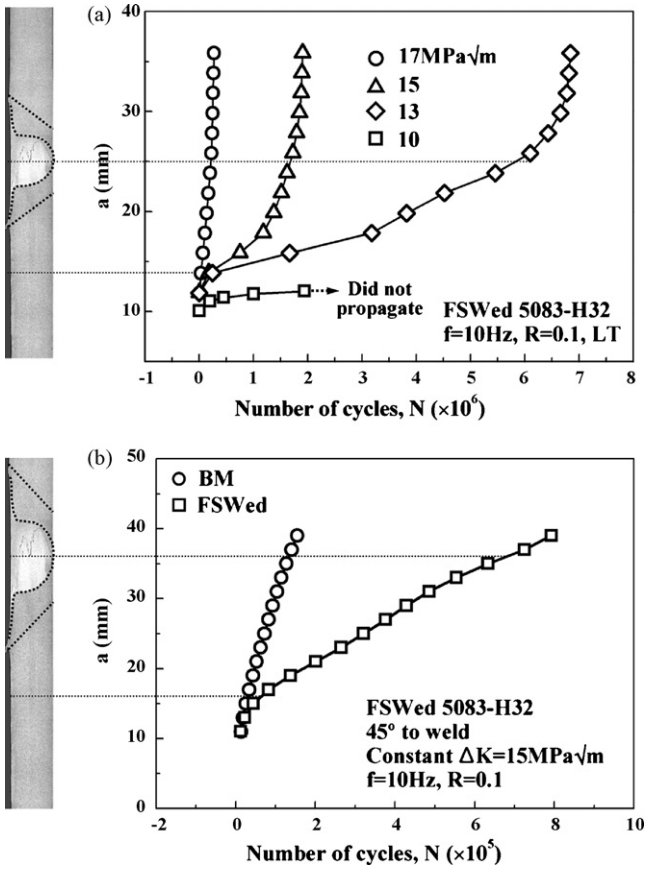

Fig. 10. Fatigue crack length, a, as a function of fatigue loading cycle, N at each applied ΔK with the crack (a) perpendicular and (b) 45°, respectively, to the weld zone for the FSWed 5083-H32 at an R ratio of 0.1.

ally affect the stage I FCP behavior. Further study is, however, required to confirm this notion.

Practically, fatigue crack may initiate in the middle portion of structural panel and propagate across the weld zone. In this study, the FCP rates for FSWed 5083-H32 and 6061-T651 specimens were measured with the crack either perpendicular or 45° to the weld zone at constant ΔK value and an R ratio of 0.1. Figs. 10 and 11 show the fatigue crack length, a, as a function of fatigue loading cycle, N at each applied ΔK with the crack (a) perpendicular and (b) 45°, respectively, to the weld zone for the FSWed 5083-H32 (Fig. 10) and 6061-T651 (Fig. 11) specimens. The macrographic cross-sectional views for the FSWed 5083-H32 and 6061-T651 specimens are also included on the left side of the graphs to identify the location where the abrupt change in the FCP rates occurs. The change in the FCP rates, as represented by the slope of a–N curve, tends to vary significantly at certain locations, the trend of which depends on the applied ΔK for both crack propagation directions and alloy specimens. At an applied ΔK of 17 MPa$\sqrt{}$m for FSWed 5083-H32 (Fig. 10(a)), for example, the FCP rates were not considerably influenced by the presence of FSW zone. At applied ΔK values of 15 MPa$\sqrt{}$m and below, the FCP rates became retarded with the crack approaching the weld zone. The fatigue crack retardation at ΔK values of 15 and 13 MPa$\sqrt{}$m began at approximately 12 mm away from the weld center, the location of which matches to the RSAZ, as defined in Fig. 4. At both applied ΔK values, the FCP rates recovered from approximately the center of the weld zone due to the residual stress relief with growing crack. At an applied ΔK value of 10 MPa$\sqrt{}$m, fatigue crack did not even propagate with the crack approaching the RSAZ. The constant ΔK fatigue test for the FSWed 6061-T651 specimens across the weld zone also showed the crack retardation far beyond the heat affected zone (HAZ) at low ΔK regime and recovery at approximately center of the weld. The residual stress measurement for the 6061-T651 specimen also suggests that the crack retardation begins with the presence of compressive residual stress in the seemingly innocuous region. The FCP behavior of FSWed 5083-H32 and 6061-T651 specimens with the crack growing 45° to the weld at constant ΔK value showed similar trend as observed in Fig. 10 for the crack growing perpendicular to the weld. In this restricted number of FCP study with the crack growing 45° to the weld, it is also observed that the crack retardation begins with the presence of compressive residual stress.

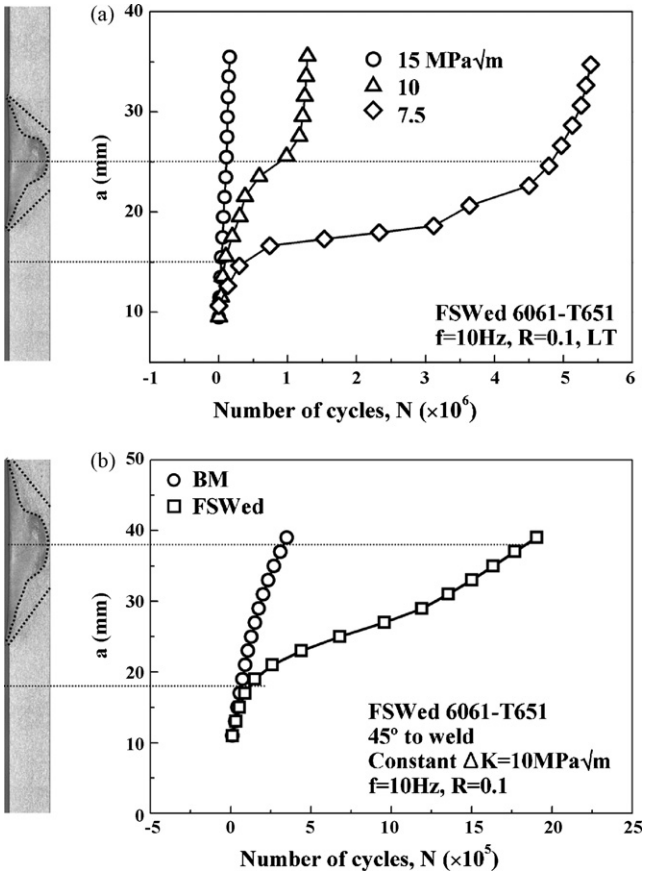

Fig. 11. Fatigue crack length, a, as a function of fatigue loading cycle, N at each applied ΔK with the crack (a) perpendicular and (b) 45°, respectively, to the weld zone for the FSWed 6061-T651 at an R ratio of 0.1.

4. Conclusions

In this study, the FCP behavior of FSWed 5083-H32 and 6061-T651 specimens were examined with the fatigue crack growing either parallel to the DXZ at variable ΔK values and an R ratio of 0.1 and 0.8, respectively, or perpendicular or 45° to the DXZ at various constant ΔK values, and the following conclusions are drawn.

1. The FCP rates of FSWed 5083-H32 and 6061-T651 specimens in the DXZ tended to be significantly lower than those in the BM at both R ratios of 0.1 and 0.8 particularly in low and intermediate ΔK regimes. The residual stress-corrected da/dN–ΔK_{corr} for the BM specimen does not completely match the da/dN–ΔK for the DXZ specimen at both R ratios for each alloy specimen. The present study suggests that the FCP behavior of FSWed 5083-H32 and 6061-T651 specimens in the DXZ is mainly determined by the beneficial compressive residual stress reducing effective ΔK and the detrimental grain refinement causing intergranular fatigue failure.
2. The constant ΔK fatigue tests either perpendicular or 45° the weld zone at an R ratio of 0.1 show that crack retardation begins with the crack approaching the residual stress affected zone at low ΔK regime. At high applied ΔK, the FCP rates are not considerably influenced by the presence of FSW zone. The present study strongly suggests that the presence of FSW zone in front of propagating crack retards the FCP rates of 5083-H32 and 6061-T651 specimens significantly in low and intermediate ΔK regimes due to the residual stress acting on the FSW zone.

Acknowledgments

This research was supported by a grant from the Center for Advanced Materials Processing (CAMP) of the 21st Century Frontier R&D Program funded by the Ministry of Science and

Technology, Korea. This work was also supported by the second stage of BK21 project.

References

[1] H.G. Salem, A.P. Reynolds, J.S. Lyons, Scr. Mater. 46 (2002) 337–342.
[2] S.G. Lim, S.S. Kim, C.G. Lee, S.J. Kim, Metall. Mater. Trans. A 35A (2004) 2837–2843.
[3] B. Heinz, B. Skrotzki, Metall. Mater. Trans. B 33B (2002) 489–498.
[4] M.W. Mahoney, G.G. Rhodes, J.G. Flintoff, R.A. Spurling, W.H. Bingel, Metall. Mater. Trans. A 29A (1998) 1955–1964.
[5] S.G. Lim, S.S. Kim, C.G. Lee, S.J. Kim, Met. Mater. Int. 11 (2005) 113–120.
[6] S.G. Lim, S.S. Kim, C.G. Lee, S.J. Kim, Metall. Mater. Trans. A 35A (2004) 2829–2835.
[7] S.G. Lim, S.S. Kim, C.G. Lee, S.J. Kim, Metall. Mater. Trans. A 36A (2005) 1977–1980.
[8] C. Zhou, X. Yang, G. Luan, Mater. Sci. Eng. A 418 (2006) 155–160.
[9] M.A. Sutton, B. Yang, A.P. Reynolds, R. Taylor, Mater. Sci. Eng. A 323 (2002) 160–166.
[10] Y.S. Sato, Y. Sugiura, Y. Shoji, S.H.C. Park, H. Kokawa, K. Ikeda, Mater. Sci. Eng. A 369 (2004) 138–143.
[11] P.S. Pao, E. Lee, C.R. Feng, H.N. Jones, D.W. Moon, Proceedings of the Fourth International Symposium on FSW, Park City, Utah, May 2003.
[12] K.V. Jata, K.K. Sankaran, J.J. Ruschau, Metall. Mater. Trans. A 31A (2000) 2181–2192.
[13] R. John, K.V. Jata, K. Sadananda, Int. J. Fatigue 25 (2003) 939–948.
[14] G. Bussu, P.E. Irving, Int. J. Fatigue 25 (2003) 77–88.
[15] K.T. Park, S.H. Myung, D.H. Shin, C.S. Lee, Mater. Sci. Eng. A 371 (2004) 178–186.
[16] J.H. Lee, H.S. Kim, C.W. Won, B. Cantor, Mater. Sci. Eng. A 338 (2002) 182–190.
[17] C.-S. Tsao, C.-Y. Chen, U.-S. Jeng, T.-Y. Kuo, Acta Mater. 54 (2006) 4621–4631.
[18] ASTM E 647 Standard, 03.01, 2002, p. 614.
[19] D. Broek, The Practical Use of Fracture Mechanics, FractuREsearch Inc., Galena, OH, USA, 1998, p. 68.
[20] R.C. Rice (Ed.), SAE Fatigue Design Handbook, third ed., Society of Automotive Engineers, Inc., Warrendale, PA, USA, 1997, pp. 332–333.
[21] J.A. Newman, Ph.D. Dissertation, University of Virginia, 2000, 141 pp.
[22] J.-Q. Su, T.W. Nelson, R. Mishra, M. Mahoney, Acta Mater. 51 (2003) 713–729.
[23] J.-Q. Su, T.W. Nelson, C.J. Sterling, Mater. Sci. Eng. A 405 (2005) 277–286.